Earth, Moon, and Planets (2005) 97: 311–329
DOI 10.1007/s11038-006-9081-y
© Springer 2006

Electronic Sputtering Analysis of Astrophysical Ices

L. S. FARENZENA, P. IZA, R. MARTINEZ,
F. A. FERNANDEZ-LIMA, E. SEPERUELO DUARTE,
G. S. FARAUDO, C. R. PONCIANO and E. F. da SILVEIRA
Departamento de Física, Pontifícia Universidade Católica, 22543-970, Rio de Janeiro, Brazil (E-mail: enio@fis.puc-rio.br)

E. SEPERUELO DUARTE
Centro Federal de Educação Tecnológica de Química de Nilópolis, 26530-060, Nilópolis, RJ, Brazil

M. G. P. HOMEM and A. NAVES de BRITO
Laboratório Nacional de Luz Síncrotron, Box 619213084-971, Campinas, SP, Brazil

K. WIEN
Guest of the Institute of Nuclear Physics, Technical University, 64289, Darmstadt, Germany

(Received 5 November 2005; Accepted 25 April, 2006)

Abstract. Experimental results on fast ion collision with icy surfaces having astrophysical interest are presented. ^{252}Cf fission fragments projectiles were used to induce ejection of ionized material from H_2O, CO_2, CO, NH_3, N_2, O_2 and Ar ices; the secondary ions were identified by time-of-flight mass spectrometry. It is observed that all the bombarded frozen gas targets emit cluster ions which have the structure $X_nR^{\pm}$, where X is the neutral ice molecule and $R^{\pm}$ is either an atomic or a molecular ion. The shape of the positive or negative ion mass spectra is characterized by a decreasing yield as the emitted ion mass increases and is generally described by the sum of two exponential functions. The positive ion water ice spectrum is dominated by the series $(H_2O)_nH_3O^+$ and the negative ion spectrum by the series $(H_2O)_nOH^-$ and $(H_2O)_nO^-$. The positive ion CO_2 ice spectrum is characterized by $R^+ = C^+$, O^+, CO^+, $O_2{}^+$ or $CO_2{}^+$ and the negative one by $R^- = CO_3{}^-$. The dominant series for ammonia ice correspond to $R^+ = NH_4{}^+$ and to $R^- = NH_2{}^-$. The oxygen series are better described by $(O_3)_nO_m{}^+$ secondary ions where m = 1, 2 or 3. Two positive ion series exist for N_2 ice: $(N_2)_nN_2{}^+$ and $(N_2)_nN^+$. For argon positive secondary ions, only the $(Ar)_nAr^+$ series was observed. Most of the detected molecular ions were formed by one-step reactions. Ice temperature was varied from ~20 K to complete sublimation.

Keywords: Cometary ice, condensed gas (H_2**O, CO_2, CO, NH_3, N_2, O_2, Ar)**, ion cluster, TOF SIMS, temperature dependence

1. Introduction

For millions or even billions of years, the Sun and other cosmic sources have bombarded with photons and fast particles the icy surface of comets,

asteroids and interplanetary grains. The most important effects of this bombardment are heating, sputtering, momentum transfer, chemical reactions and ion implantation. The heating generates mechanical stress, induces material phase changes (sublimation in particular) and speeds up chemical reactions. The sputtering by solar wind or by cosmic rays produces nanometric craters on the body surface and the ejection of atoms and molecules with velocities often greater than the local escape velocity. The momentum transfer of the radiation or of the solar wind is especially relevant for light target objects such as the particles constituting the cometary coma. Chemical reactions are triggered by UV Sun light and by fast particles (electrons, protons and heavier ions), which are very efficient ionizing agents. Ion implantation – besides contributing to chemical reactions – changes the structural and elemental profile of icy surfaces, modifying physical properties such as crystallinity, color or reflectance of electromagnetic waves. The knowledge of photoionization cross sections and sputtering yields is essential for the modeling of the processes occurring on the surface of comets and of other bodies not protected by a dense atmosphere. Such fundamental data base can be obtained in laboratory by simulating the impact of solar photons and particles on ice targets.

The effects of energetic (keV to GeV) particle bombardment on cosmic ice or grains have been studied for a long time (Johnson, 1990; Johnson, 1998; Strazzula and Palumbo, 1998; Cottin et al., 1999; Hudson and Moore, 2001; Madey et al., 2002; Johnson et al., 1983; Strazzulla et al., 1991; Moore et al., 1991; Brucato et al., 1997; Kobayashi et al., 1995; Johnson, 1999; Baragiola et al., 2003; Collado et al., 2004; Farenzena et al., 2005; Ponciano et al., 2005; Farenzena et al., 2006; Martinez et al., 2006, in press; Ponciano et al., 2006; Baba et al., 2005; Gomis and Strazzulla, 2005; Wagner et al., 1993; Tonuma et al., 1994; Matsuo et al., 1994). Survey on the subject can be found in the reviews of Johnson (1990, 1998), Strazzulla and Palumbo (1998), Cottin et al. (1999), Hudson and Moore (2001) and Madey et al. (2002). Erosion yields for several frost gases are reported by Johnson et al. for 1.5 MeV He^{+} beam (Johnson et al., 1983) and by Japanese researchers using 1.5 MeV/u Ar^{13+} projectiles (Tonuma et al., 1994; Matsuo et al., 1994; Tawara et al., 1991). For water ice sputtering in particular, Baragiola et al. (2003) have updated the knowledge on this abundant cometary substance.

A project to study the secondary ion emission from several condensed gases is underway at the Van de Graaff Accelerator of the Pontifical Catholic University (PUC, Rio de Janeiro) (Collado et al., 2004; Farenzena et al., 2005; Ponciano et al., 2005) and at the Laboratório Nacional de Luz Síncrotron (LNLS, Campinas) (Farenzena et al., 2006; Ponciano et al., 2006). The project covers the analysis of the prompt secondary ion emission induced by 0.2–2 MeV nitrogen beam, ~65 MeV fission fragments and by 10–100 eV photons (UV radiation), at different ice temperatures. Furthermore, it is in

progress the analysis of the residue at room temperature of ice mixtures bombarded by UV light for a long period of time. In the first stage of this project, the focus is set on three points: (i) the determination of total secondary ion yields (i.e., the total number of ions emitted from the ice per projectile impact), (ii) the analysis of ion cluster emission of pure ices (mass distribution of the ionized clusters) and (iii) identification of new chemical species produced by the irradiation on a mixture of ices. Some findings on H_2O, CO_2 and CO have been published recently (Collado et al., 2004; Farenzena et al., 2005; Ponciano et al., 2005; Farenzena et al., accepted). Complementing the analysis of MeV nitrogen ion impact on frozen H_2O + CO_2, the present article reports new experimental results on electronic sputtering of ions produced by the impact of ^{252}Cf fission fragments on frozen H_2O, CO, CO_2, NH_3, N_2, O_2, and Ar. It is reminded that Ba^{15+} is a typical ^{252}Cf fission fragment and that 65 MeV is its average energy after traversing the sealing foil of the radioactive source.

2. Fundamental Background

One of the crucial physical quantities that rule the sputtering process (and therefore the amount of target material ejected in the bombardment) is the rate of the projectile kinetic energy deposited in the target. This quantity, called stopping power (S), is defined as the energy withdrawn from the projectile per length unit of its trajectory inside the target. For projectile velocities below ~200 km/s (for protons) to ~1000 km/s (for heavy ions), the projectile interacts mainly with target atomic nuclei, so that S is called nuclear stopping power (S_n). Above these velocities, the predominant interaction occurs with target electrons and the transferred energy rate is given the electronic stopping power, S_e. Figure 1 presents the total stopping power ($S = S_n + S_e$) for H, He and Ba ions on water ice, as a function of the projectile velocity. Protons and α particles, having a typical solar wind velocity of 400 km/s (~1 keV/u), as well as cosmic rays (100 keV–1 GeV), interact with water ice mainly via target electrons and their energy loss is essentially described by S_e. In general, experiments with Van de Graaff accelerators are performed with ~MeV particles; Plasma Desorption Mass Spectrometry (PDMS) technique measurements (Collado et al., 2004) employ ^{252}Cf fission fragments (FF) as projectiles, whose representative energies (on target) are ~65 MeV of barium ions. Therefore, electronic sputtering results obtained with these two experimental methods can be used to analyze the solar wind and cosmic rays effects.

Figure 1 shows another important point. The stopping power of fission fragments is about two orders of magnitude higher than that of H or He at solar wind velocities. Induced ion desorption yields (which roughly behaves

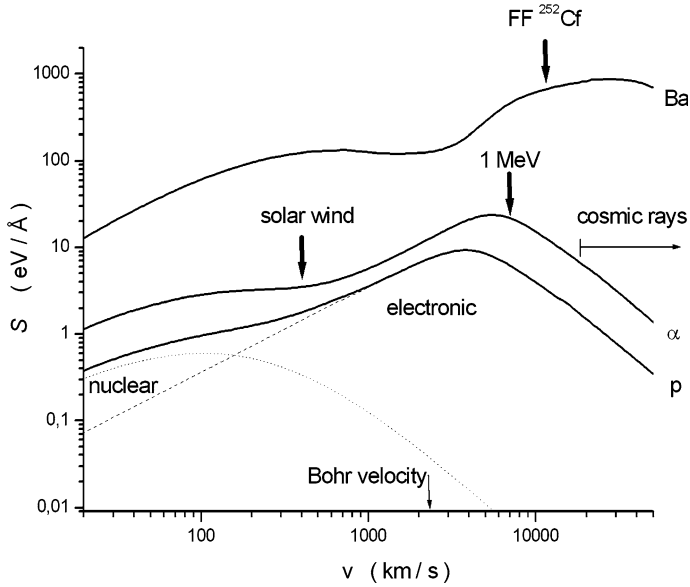

Figure 1. The total stopping power of protons, α particles and barium projectiles on water ice. For protons, the dot and dash lines represent the nuclear and the electronic stopping power, respectively. Ba is a common fission fragment (FF) of the ^{252}Cf; its velocity (energy of ~65 MeV) after leaving the radioactive source employed is indicated by the arrow. Velocities of 1 MeV α particles and of a typical solar wind are also indicated. Note that the electronic stopping power values of the solar wind and cosmic rays are much greater than the corresponding nuclear stopping power values.

as S_e^n, n varying from 1 to 3) and chemical reaction rates are then strongly enhanced, increasing sensitivity of experimental methods and drastically reducing time of measurements. In order to scale down FF sputtering yields into solar winds velocities and for light projectiles (H or He), the following results are useful. The H_2O sputtering yield of He^+ is one order of magnitude higher than H^+ at the same velocity (Baragiola et al., 2003) and their stopping power ratio is 2–3 at solar wind velocities, suggesting $n \sim 2$–2.5. As $S_{FF} \sim 100\ S_{He}$ and $Y_{He} \sim 2$ molec/ion, the total sputtering yield produced by FF impact are expected to be $\sim 10^5$–10^6 molec./ion. Both the higher projectile flux and the higher desorption yield of the FF projectiles make it possible to study in laboratory time what nature needs thousands or million of years to achieve.

Electronic stopping powers are calculated through codes such as SRIM (1996) or CasP (Grande and Schiwietz, 1998). Important characteristics of S_e are its dependence on q^2 and its maximum value at $\sim Z_p^{3/2}\ V_{Bohr}$ (where q and Z_p are the projectile charge and atomic number, $V_{Bohr} = 2200$ km/s). Many works have succeeded in connecting ion desorption yields, Y, with S_e for specific cases; see review by Le Beyec (1992) and references therein. In

particular, it has been found that $Y \alpha q^3$ for positive hydrogen secondary ions, $Y \alpha q^2$ for negative secondary ions, $Y \alpha q^{3.5}$ for N_2 adsorbed on carbon (Caron et al., 2001) and projectile velocity corrections of Y (Pereira and da Silveira, 2000).

3. Mass Spectra and Electronic Sputtering Yields

3.1. Experimental setup

The sample preparation, experimental setup and data acquisition treatment are described in references (Collado et al., 2004; Farenzena et al., 2005, accepted). Briefly, secondary ions were analyzed by time-of-flight (TOF) mass spectrometry. ^{252}Cf fission fragments with energies of about 65 MeV were used to induce positive and negative ion desorption (see, for instance, Wien, 1997). A quadrupole mass spectrometer was included to monitor the residual gas simultaneously. The base pressure of the chamber was about 2×10^{-8} mbar, which increased by one or two orders of magnitude when the gas was introduced in the chamber for condensation. The target temperature was determined by a thermocouple having a reference at 0 °C, so that the yield of the secondary ions could be followed during the warming up period. The typical condensation temperature is around 25–30 K, and maximum ice thickness was in the μm range. The obtained ^{252}Cf-PDMS-TOF mass spectra and the total yields of the most abundant astrophysical ices are reported below.

3.2. H_2O ice

Water, carbon monoxide, ammonia and methane are usually the most common molecules present on comets. Water ice is in general the most abundant component in astrophysical ices, the other components being frozen or trapped inside a porous water ice structure. When a comet is closer than 7 AU to the Sun, the ices start to sublimate according to their sublimation temperature (Capria 2002), the CO molecules appearing first (see Figure 2). Closer than 4 AU, phase transformations of the ice matrix occur and the flux of the volatiles increases due to the release of the trapped gases. During this process, other molecules (e.g., H_2O) can be dragged with the volatile gases. We could monitor the sublimation of the H_2O, CO and NH_3 ice mixture by measuring the residual gas pressure in the chamber with a quadrupole mass spectrometer. It was observed first the sublimation of the gases according to their sublimation temperature with the dragging of other molecules and, after, the release of trapped gases during structural changes in

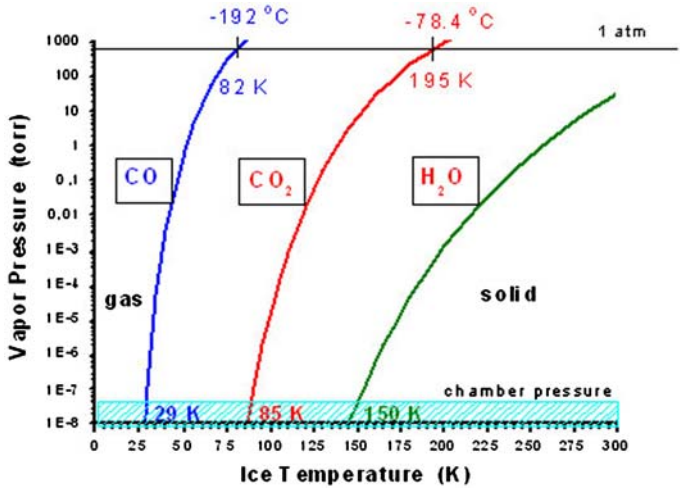

Figure 2. Sublimation temperature of ices for different gas pressures.

the ice matrix. Unfortunately, this kind of measurement cannot be used (in our experiment) to determine the sputtering yield of neutrals because the flux of the fission fragment beam is extremely low. A more complete discussion of quadrupole mass spectrometry data is presented elsewhere (Martinez et al., accepted) for NH_3/H_2O ice.

Typical PDMS mass spectra of water ice are shown in Figure 3a and b, for positive and negative ions, respectively. Note in particular that the series of ion clusters $(H_2O)_nH_3O^+$ and $(H_2O)_nOH^-$ have the highest yields. It has been observed that, as the cluster mass increases, the yields of both series decrease and can be fitted by the sum of two exponentials (Collado et al. 2004; Martinez et al., accepted), one decaying fast (F) and the other decaying slowly (S):

$$Y(m_n) = Y_0^F \exp(-k_m^F m_n) + Y_0^S \exp(-k_m^S m_n) \quad (1)$$

where m_n is the mass of the cluster n, $k_m^F = 0.045$ u^{-1} is the fast-decay constant and $k_m^S \sim k_m^F/5 = 0.008$ u^{-1} is the slow-decay constant for the positive ion series. We also measured that $k_m^F = 0.035$ u^{-1} and $k_m^S = 0.009$ u^{-1} for the negative ion series, which are about the same as the positive ion constants. Except for close to the sublimation temperature, the total yield of the series, Y_T ($\sim Y_0^F/k_m^F + Y_0^S/k_m^S$), and the shape of the distribution $Y(m_n)$ depend moderately on ice temperature. This fact is illustrated in Figure 4a where a 3-dimentional plot shows a sequence of mass spectra corresponding to the water ice warming up (from region A to region B). The mass spectrum in Figure 4b is the sum of the last 10 spectra of Figure 4a, acquired just before the fast ice sublimation (region B represents the spectra obtained when the ice

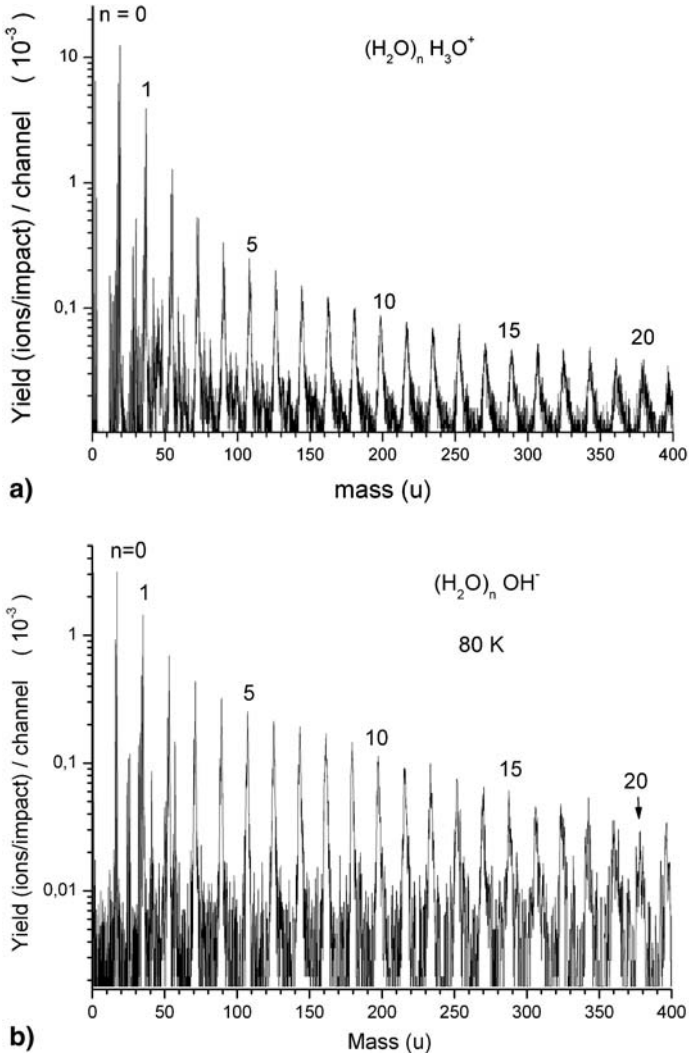

Figure 3. ^{252}Cf FF – TOF mass spectra of (a) positive and (b) negative secondary ions of water ice.

temperature varied from 140 to 150 K). Figure 4c corresponds to the first 10 spectra of the Figure 4a, at ice temperatures from 30 to 35 K. Approaching the sublimation temperature at ~150 K and before the ice layer becomes too thin, the yields of the large clusters decrease while that of the light ones increase. Since the cluster binding energy decreases when n increases, large ion clusters are more fragile and dissociate into smaller ones, as shown in Figure 5. Such behavior also allows us to interpret the steeper exponential, labeled as "F", as representing the fragmentation of large clusters into small

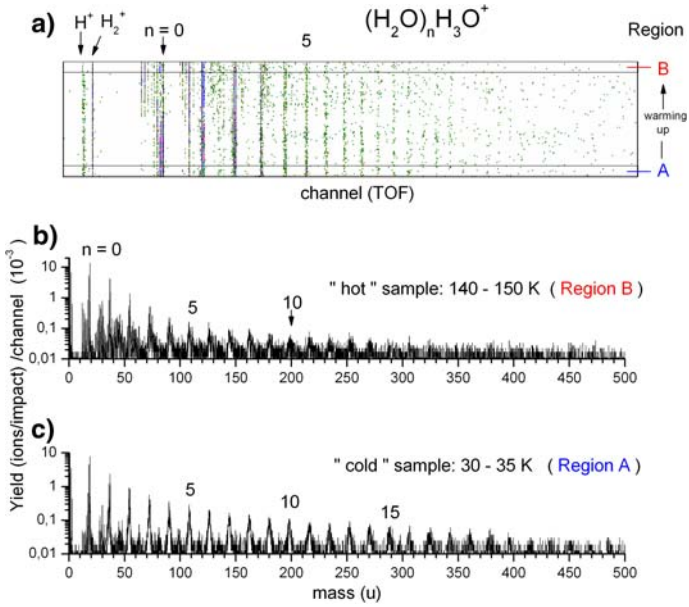

Figure 4. PDMS mass spectra of H_2O positive ions for several ice temperatures. (a) 3-dimensional plot, where abscissa is the ion cluster mass and ordinate is ice temperature; (b) sum of 10 mass spectra of the high ("hot") temperature region; (c) idem for low ("cold") temperature region. Note that peaks of large clusters are less defined in the "hot" sample spectrum, indicating instability.

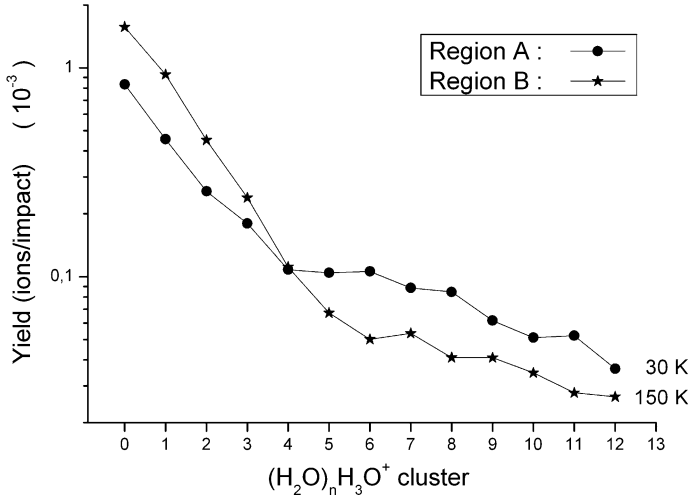

Figure 5. Comparison of the yield distributions of H_2O secondary ions at low and high temperatures. Data are the same as Figure 4b. The yields of small clusters increase at high temperatures due to fragmentation of large clusters.

ones (see Eq. 1). Another argument in this direction is the absence of the fast-decay exponential for the impact of light projectiles (Collado et al., 2004).

Another characteristic of the water ice ion desorption is the behavior of peaks relative to masses 18 u (H_2O^+) and 19 u (H_3O^+): their yield ratio changes dramatically above and below the sublimation temperature. Protonation seems to be very efficient on the bombarded ice surface, in contrast to the situation of a lower density of water molecules adsorbed on the substrate at temperatures higher than the sublimation temperature. The desorption yields of the H^+, $H_2{}^+$ and H^- ions are relatively high, while those of $H_3{}^+$, O^+, OH^+, $O_2{}^+$, O^- and OH^- are moderate (Collado et al., 2004).

Water ice sputtering by H^+, He^+, O^+, Ar^+ ions for incident energies lower than 100 keV/atom and for 20–150 K ice temperatures has been reviewed recently by Baragiola et al. (2003). They report total sputtering yield (i.e., ion plus neutral yields) in the range 3–80 water molecules/projectile; the total yield of ~100 water molecules/projectile was quoted by Johnson for 240 keV N^+ ion impact on ice (Johnson, 1990). These results may be compared with the ionic total electronic sputtering yield of about 10 molecules/projectile, exclusively for ion desorption induced by FF (see Section 2 and Table I), i.e., a total neutral molecular yield of ~ 10^5, remembering that the neutral molecular yield can be 2–5 orders of magnitude higher than the ion yield. Johnson et al. reported the yield of 8 neutral water molecules for 1.5 MeV He^+ beam for ice at 10 K and suggested that such low value was related to the relatively high molecular binding energy (0.52 eV) of water (Johnson et al., 1983).

3.3. CO ICE

CO has the lowest sublimation temperature, after the diatomic molecules H_2, N_2, O_2 and after the noble gases He, Ne and Kr. When comets approach the Sun at distances ~7 AU, CO is the first abundant substance to sublimate and it becomes the main constituent of their coma (Caron et al., 2001). When approaching the Sun (<4 AU), the abundance of CO is enhanced by release of trapped gases in the water ice structure. At distances shorter than ~2 AU, since small grains and other compounds have already been released from the nucleus, CO starts to be produced directly in the coma by thermal destruction of some of these materials (Capria, 2002). As a consequence, the CO abundance may reach up to 20% of water abundance (Greenberg, 2002).

Positive and negative ion PDMS spectra of CO ice are presented in Figure 6a and b, respectively. The positive and negative ion cluster series were identified and are represented by the chemical expressions $C_n{}^+$, $(CO)_mC_n{}^+$, $C_n{}^-$ and $(CO)_nO^-$. The dominant series in the positive ion spectrum is $(CO)_2C_n{}^+$, whose decay constant is $k_m{}^S = 0.011$, close to the water ice low

TABLE I

Total ion desorption yield (Y_T) for sputtering of ice by ^{252}Cf fission fragments. Desorbed molecules per impact means the average number, per projectile, of target ice molecules (M = 18) emitted as the secondary ions in the cluster series ($=\Sigma Y(m)m/M$). Yields for specific and hybrid desorbed ions can be found in references (Collado et al., 2004; Farenzena et al., 2005; Ponciano et al., 2005; Farenzena et al., 2006; Martinez et al., 2006, in press). Erosion yields for 1.5 MeV He^+ beam are given in Johnson et al. (1983)

Target (ice)	Ion series	Approximate temperature (K)	Desorption yield Y_T (ions/impact)	Desorbed molecules/impact	Reference
H_2O	$(H_2O)_nH^+$	150	0.58	1.5	Collado et al. (2004)
H_2O	$(H_2O)_nH^+$	80	1.17	3.9	Collado et al. (2004)
H_2O	pos*	80	2.73	9.1	Collado et al. (2004)
H_2O	pos* N^+	80	0.084	0.35	Collado et al. (2004)
H_2O	$(H_2O)_nOH^-$	80	0.021	0.070	Collado et al. (2004)
H_2O $n \leq 10$	neg*	80	0.11	0.37	Collado et al. (2004)
H_2O $n \leq 20$	neg*	80	0.17	0.97	This work
CO	$(CO)_mC_n{}^+$	30	2.78	–	Collado et al. (2004)
CO	$(CO)_mC_n{}^-$	30	0.031	–	Collado et al. (2004)
CO_2	pos*	80	2.6	3.5	Farenzena et al. (2005)
CO_2	neg*	80	1.12	–	Farenzena et al. (2005)
CO_2 + 9% H_2O	pos* N^{2+}	90	0.35	0.91	Farenzena et al. (2005)
CO_2 + 5% H_2O	neg* N^{2+}	90	0.06	0.11	Farenzena et al. (2005)
NH_3	pos*	30 – 70	1.11	5.1	Martinez et al. (2006)
NH_3	neg*	30 – 70	0.58	3.8	Martinez et al. (2006)
N_2	$(N)_n{}^+$	30	2.18	15	This work
O_2	pos*	30	1.66	3.1	This work
O_2	neg*	30	0.40	1.1	This work
Ar	$(Ar)_n{}^+$	30	1.83	4.6	This work

pos* (neg*) Corresponds to contribution of all positive (negative) ions in the spectrum.
N^+ Data obtained with N^+ beam with 0.85 MeV.
N^{2+} Data obtained with N^{2+} beam with 0.85 MeV.

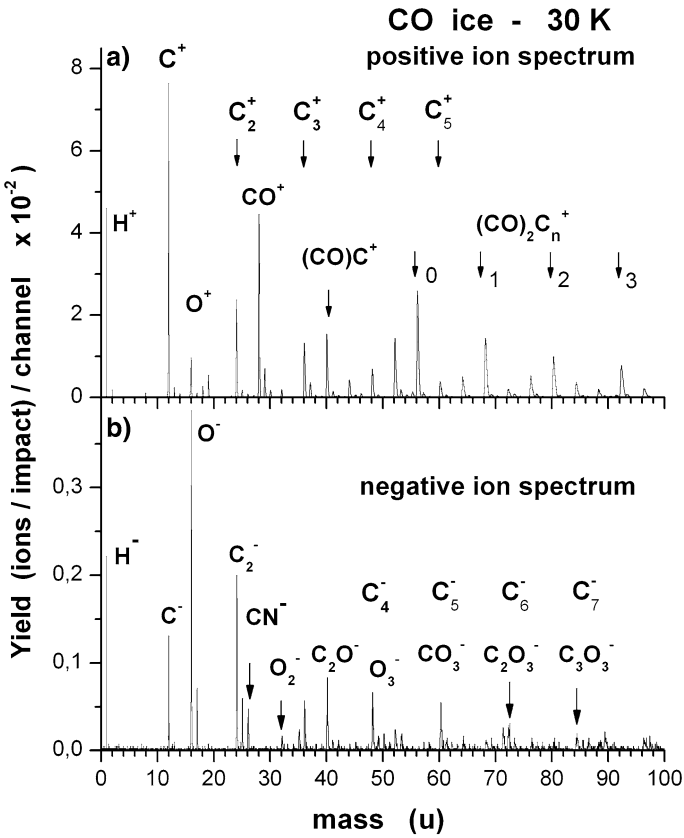

Figure 6. (a) Positive and (b) negative PDMS spectra of CO ice.

decay constant. The total positive ion yield of CO secondary ions is two orders of magnitude higher than that of the negative ion (Table I). Tonuma et al. have analyzed the ion sputtering of CO ice by 1.5 MeV/u Ar^{13+} and reported similar results: (i) the observed dominant negative ion cluster series is the C_n^- and (ii) the positive ion series have the $(CO)_nR^+$ structure, where $R^+ = C_m^+$, O^+, CO^+ and O_2^+ (Tonuma et al., 1994).

3.4. CO_2 ICE

Oxygen and carbon are, respectively the third and the fourth most abundant elements in the Universe, just after hydrogen and helium. Both atoms are very reactive and the CO_2 molecule is expected to be formed. In interstellar ices, CO_2 may be more abundant than CO. For the Hyakutake and

Hale-Bopp comets, measurements of *gaseous* compounds have indeed shown that CO is more abundant than CO_2 (Cottin et al., 1999).

Figure 7a and b show the mass spectra of positive and negative secondary ions of a CO_2 ice target. It should be noted in Figure 7a that the dominant peak is O_2^+, which means that the bombardment of CO_2 is releasing oxygen from the fragmentation into CO + O. The positive ion CO_2 ice spectrum is complex, and the chemical stoichiometry of the main emitted products may be classified into two series: the $(CO_2)_nR^+$, with the radical $R^+ = C^+, O^+, CO^+, O_2^+$ or CO_2^+, and the $(CO)_n^+$.

The negative ion spectrum of CO_2 is dominated by O^- and by the series $(CO_2)_nCO_3^-$, as seen in Figure 7b. Note that the reaction $CO_2 + O^- \rightarrow CO_3^-$ will consume the available oxygen anion. When mixing CO_2 and H_2O molecules in the ice, the most intense positive hybrid cluster ions are COH^+, $(CO_2)_mH^+$, $(CO_2)_m(H_2O)_nH^+$, while the most intense negative hybrids are

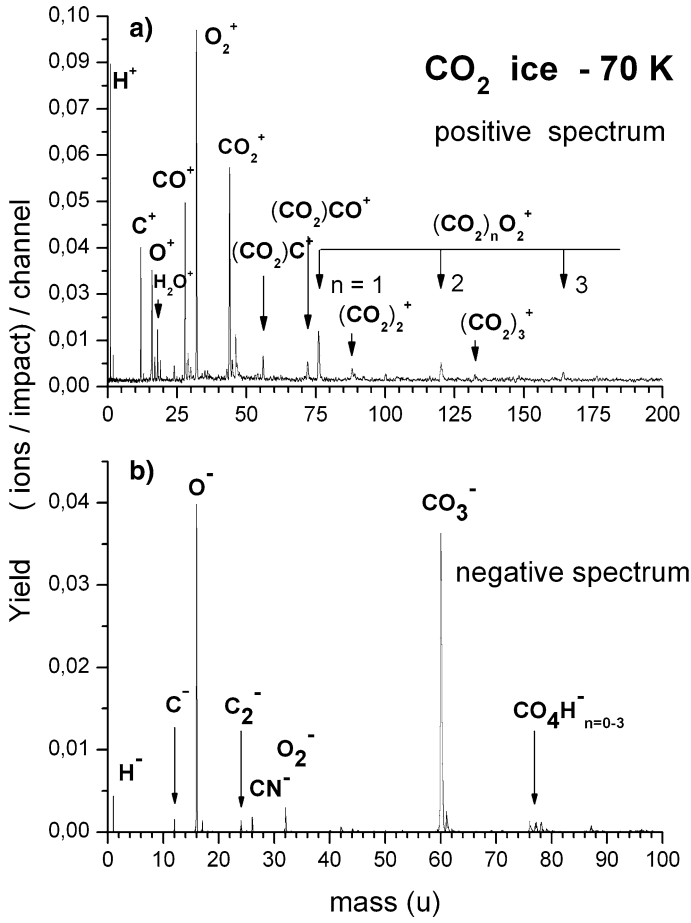

Figure 7. (a) Positive and (b) negative PDMS spectra of CO_2 ice.

$(CO_2)OH^-$, $CO_4H_m^-$ and the cluster series. By far, most of the measured molecular ions have been formed by one-step reactions (except $CO_4H_m^-$) (Ponciano et al., 2005).

A comparative ^{252}Cf-PDMS-TOF analysis between ion sputtering from CO and CO_2 ices is described in Ponciano et al. (2006). It should also be mentioned that Tawara et al., using 1.5 MeV/u Ar^{13+} projectiles and a double-focusing sector magnet, obtained positive and negative mass spectra of cluster ions emitted by CO_2 ice: the reported series have also the $(CO_2)_nR^{\pm}$ structure, where $R^{\pm}$ are the same radicals found in the current measurements, the O_2^- included (Tawara et al., 1991).

3.5. NH_3 ICE

Ammonia ice has been suggested to be present in interstellar clouds (1–10%/water), in cold satellites such as Charon and in several cometary comae (0.1–0.55%/water) (Cottin et al., 1999; Hudson and Moore, 2001). Since N_2 is low reactive, ammonia is expected to play an important role in the synthesis of cosmic amines. Excited by UV photons or by fast particles, NH_3 has the tendency to protonate into NH_4^+ or to produce anions such as NH_2^-, NH^- and N^-, enhancing chemical reactions. The positive and negative secondary ion spectra shown in Figure 8a and b, respectively, illustrate these characteristics: NH_3 molecules aggregate around the NH_4^+ anion, generating the positive ion $(NH_3)_nNH_4^+$ cluster series and around the de-protonated NH_2^- cation, generating the negative ion $(NH_3)_nNH_2^-$ cluster series.

Illustrating a desorbed cluster structure, Figure 9 shows the species $(NH_3)_{16}NH_4^+$. The ion NH_4^+ is placed at the center of the system and holds the ion charge. N neighbor atoms are linked to each of its four H atoms by the so called hydrogen bridge. By the same process, four other ammonia molecules are linked to these, yielding a total of 16 molecules attached to the central NH_4^+ ion. A detailed structural characterization of the positive, neutral and negative ammonia cluster series (ranging from n = 1–8) using density functional theory (DFT) can be found in (F.A. Fernandez-Lima et al., submitted).

3.6. N_2 ICE

N_2 is virtually absent in comets although the element N is relatively common in the Universe, about one order of magnitude less abundant than O and few times less than C. Its low sublimation temperature (34 K at 10^{-8} mbar) could be an explanation for its low occurrence as ice, although CO sublimates at a lower temperature. Nitrogen appears more often in other compounds such as

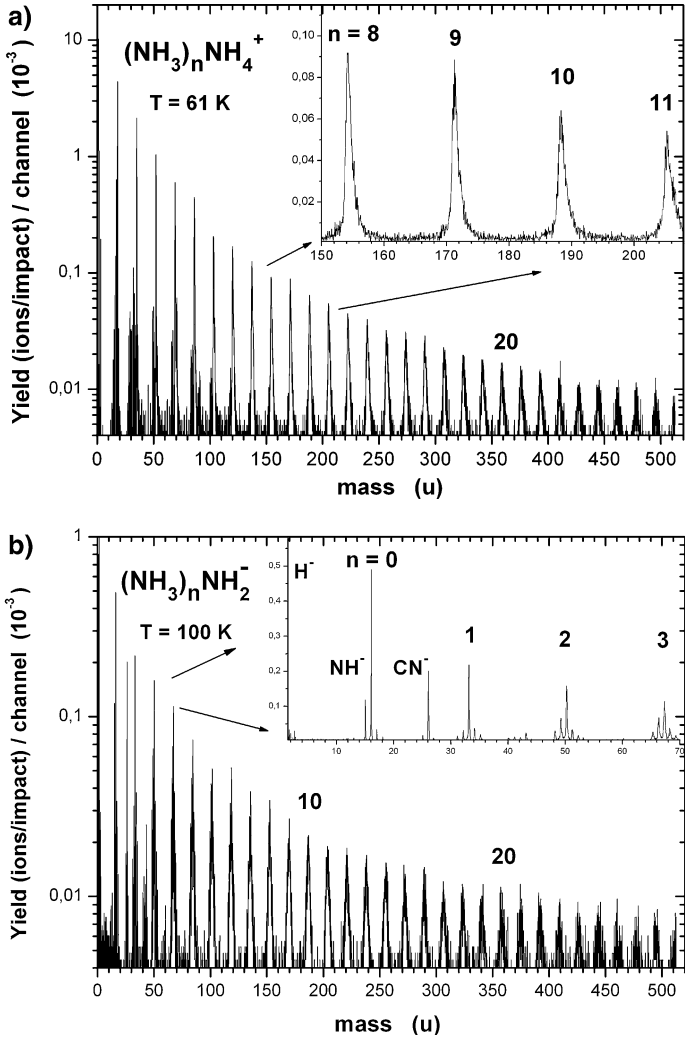

Figure 8. (a) Positive and (b) negative PDMS spectra of NH_3 ice.

NH_3, HCN or OCN. As ice, N_2 has been identified in very cold bodies, namely Triton, Pluto and Charon (Hudson and Moore, 2001).

Figure 10 shows a PDMS spectrum of positive secondary ions emitted from N_2 ice. Two features characterize the ion desorbed yield distribution of N_n^+ clusters: the fast and slow decay regime, for low and high masses, respectively, and the odd/even periodicity. In fact, the latter property suggests the occurrence of two series: $(N_2)_nN^+$ and $(N_2)_nN_2^+$, in which the seeds N^+ and N_2^+ appear explicitly. Carbon contamination in nitrogenated compounds gives rise very easily to CN^- secondary emission in negative ion spectra.

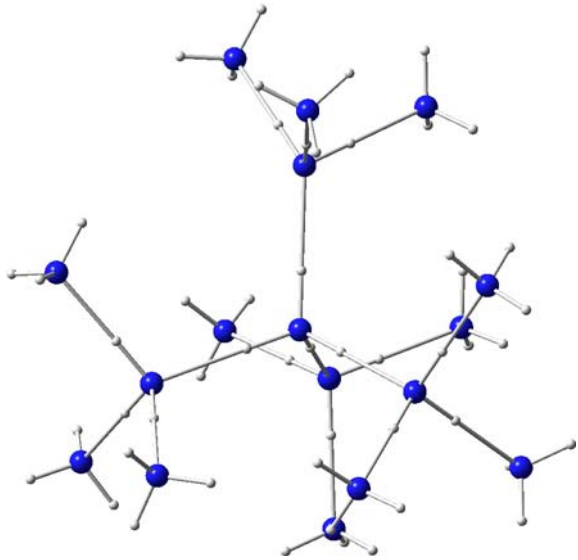

Figure 9. Structure of the $(NH_3)_{16}NH_4^+$ ion cluster. Note the central NH_4 ion is linked by hydrogen bonds to four NH_3 molecules. The ratio of the distances of the H to the two N atoms is about 1.2/1.6.

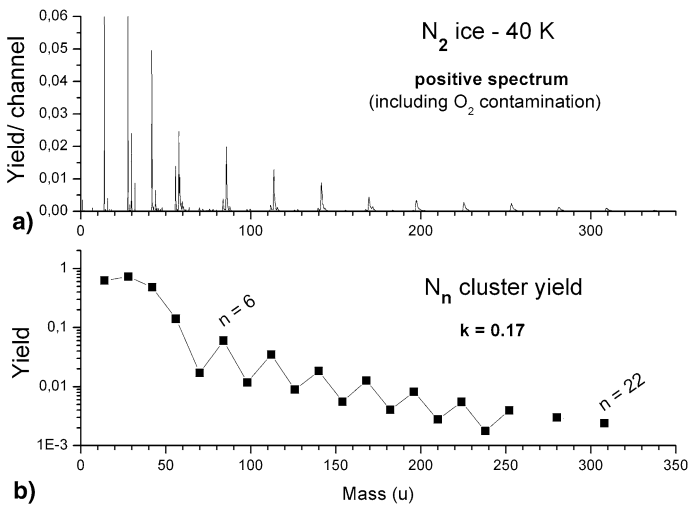

Figure 10. (a) Positive PDMS spectra of N_2 ice and (b) N_n as a function of the cluster size.

3.7. O_2 ICE

Oxygen is the third most common element in the solar nebula, placed just below hydrogen and helium. However, the O_2 molecule is relatively rare, due to the high reactivity of oxygen with other elements, especially with carbon

(producing CO and CO_2), hydrogen (H_2O) and nitrogen (NO). The formation of the O_2 or the O_3 molecules usually requires an endoergic process, such as photosynthesis. So far, O_2 has not been observed in the cometary comae (Cottin et al., 1999), but its presence has been reported in some satellites such as Ganymede or Rhea (Hudson and Moore, 2001). Analyses concerning astrophysical aspects of frozen O_2 were discussed by Bahr (2001).

Figure 11a and b present the secondary ion yield of O_2 ice for positive and negative ions, respectively. The ratio of total yields for positive/negative ions is about 4, compared with ~25 for water and ~90 for CO, a consequence of the high electron affinity of oxygen. Note also that there is a 3n periodicity in the O_n positive and negative ion cluster yield distributions, indicating that the ozone subgroup O_3 is occurring in the structure of both distributions. Such high production of ozone is not a surprise if one bears in mind that UV from the Sun is very efficient in forming this molecule in the higher atmosphere of the Earth. Simultaneously with the formation of the $(O_3)_nO_m^+$ series, where m = 1, 2 or 3, the presence of $(O_3)_nN_2^+$ and $(O_3)_nNO^+$ series, attributed to adsorbed N_2 molecules (from small air leakages in the system) on the O_2 ice layer is also observed. The fast and slow decay constants for positive (or negative) ion series are $k_m^F = 0.05$ and $k_m^S \sim k_m^F/10 = 0.005$, respectively.

3.8. Ar ICE

Noble gases are supposed to be rare in comets. He and Ne are very abundant in the Universe but have a sublimation temperature too low to condense in

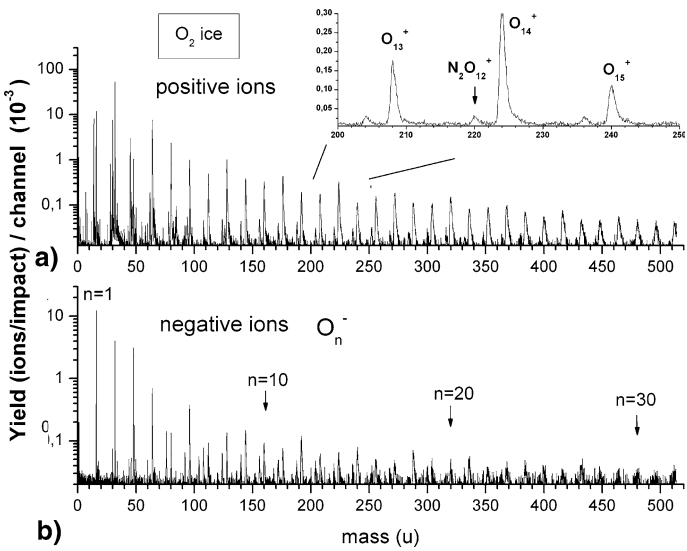

Figure 11. Positive and negative PDMS spectra of O_2 ice. Mass peaks correspond to O_n^+ and O_n^-, respectively.

active comets: this constrains their presence as trapped molecules (Notesco et al., 2003). Xe and Kr are very low abundant in general. Ar is the noble gas most likely to exist as ice in comets, since it lies in a compromising situation: its occurrence is as important as that of Si or Fe and it condenses in the range of 30–40 K.

Figure 12 shows the positive mass spectrum of Ar ice. Although it is a noble gas, the yield distribution of its desorbed ion clusters is very similar to the other ices analyzed: $k_m^F = 0.02$ and $k_m^S = 0.002$, corresponding to the ratio $k_m^F/k_m^S = 10$.

4. Conclusions

In this work, the bombardment of condensed gases of astrophysical relevance by fast projectiles (above Bohr velocity) was analyzed: the goal is to simulate the interaction of the solar wind or cosmic rays with the cold surface of interplanetary grains, comets or satellites having low pressure atmosphere or haze. In the experiments, the total mass removed as ionized material, the total number of the sputtered ions (yield) and the number of each ionized species emitted per projectile impact were determined. Measurements were done for seven ices and the desorbed ions were identified by PDMS-TOF mass spectrometry. In this technique, acquisition is performed in an event-by-event basis, i.e., by counting single ions that are emitted in each projectile impact.

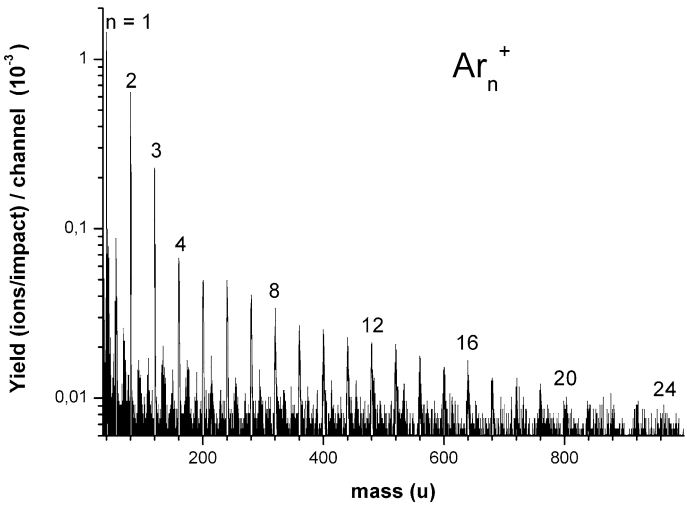

Figure 12. Positive PDMS spectra of Ar ice.

The results are summarized in Table I. Typically, 2 to 3 ions are emitted on average by impact of a Ba projectile on ice. Due to the high velocity of the projectile, secondary electrons are produced and emitted from its nuclear track. The impact site becomes positively charged and therefore the yield of positive secondary ions is higher than that of the negative ones. We have found that this ratio varies strongly according to the ice species: it is about 90 for CO and 25 for water, while it is only 4 for oxygen and 2 for CO_2 and NH_3. This is possibly related with the high electron affinity of the CO_3^- and NH_2^- molecules.

Another finding concerns the mass distributions of the emitted ions: they are very similar for all the ices measured. Typically, the secondary ions are emitted as clusters with the structure as $X_n\ R^{\pm}$, where $R^{\pm}$ is a positive or negative charged central core and X_n symbolizes n neutral ice molecules, X, surrounding the core. This structure is illustrated for the ammonia cluster $(NH_3)_{16}NH_4^+$. We also found that the mass distribution decreases exponentially and very fast up to $n \sim 5$ and keeps decreasing exponentially – but slowly – for $n > 5$. Since the absolute yield of large clusters changes with ice temperature, we propose that: (i) the fast-decay (F) regime is associated to the molecular sputtering which occurs at the extremity of the infratrack (where the local high temperature does not depend on the ice temperature), followed by recondensation forming (small) clusters and (ii) the slow-decay (S) regime is associated to the sputtering produced around the infratrack, from where (small or large) cold pre-formed clusters are emitted. Theoretical models are needed to describe these processes.

Acknowledgments

The authors acknowledge the Brazilian Agencies CNPq, Fapesp, Faperj and CLAF.

References

Baba, Y., Sekiguchi, T., and Shimoyama, I.: 2005, *Surf. Sci.* **593**, 324–330.

Bahr, D. A.: 2001, PhD Thesis, Univ. of Virginia, UMI # 9987221, and articles therein.

Baragiola, R. A., Vidal, R. A., Svendsen, W., Schou, J., Shi, M., Bahr, D. A., and Atteberry, C. L.: 2003, *Nucl. Instr. Meth. Phys. Res. B* **209**, 294–303.

Brucato, J. R., Castorina, A. C., Palumbo, M. E., Satorre, M. A., and Strazzulla, G.: 1997, *Planet. Space Sci.* **45**, 835–840.

Capria, M. T.: 2002, *Earth Moon Planets* **89**, 161–177.

Caron, M., Clouvas, A., Neugenbauer, R., Potiriadis, C., and Rothard, H.: 2001, *Phys. Scripta* **T92**, 205–207.

Collado, V. M., Farenzena, L. S., Ponciano, C. R., da Silveira, E. F., and Wien, K.: 2004, *Surf. Sci.* **569**, 149.

Cottin, H., Gazeau, M. C., and Raulin, F.: 1999, *Planet. Space Sci.* **47**, 1141.

Farenzena, L. S., Collado, V. M., Ponciano, C. R., da Silveira, E. F., and Wien, K.: 2005, *Int. J. Mass Spectrom.* **243**, 85–93.

Farenzena, L. S., Martinez, R., Iza, P., Ponciano, C. R., Homem, M.G.P., Naves de Brito, A., da Silveira, E. F. and Wien, K.: *Int. J. Mass Spectrom.* **251**, 1–9.

Gomis, O. and Strazzulla, G.: 2005, *Icarus* **177**, 570–576.

Grande, P. L. and Schiwietz, G.: 1998, *Phys. Rev.* **A58**, 3796: code Convolute approximation for swift Particles – CasP, available at http://www.hmi.de/people/schiwietz/casp.html.

Greenberg, J. M.: 2002, *Surf. Sci.* **500**, 793–822.

Hudson, R. L. and Moore, M. H.: 2001, *J. Geophys. Res.* **106**, 33275–33284.

Johnson, R. E.: 1990. *Energetic Charged Particle Interactions with Atmospheres and Surfaces*, Springer Verlag, Heidelberg.

Johnson, R. E.: 1998, in B. Schmitt, C. De Bergh and M. Festou (eds.), *Solar System Ices*, Kluwer Academic Press, Netherland, p. 303.

Johnson, R. E.: 1999, *Braz. J. Phys.* **29**, 444–449.

Johnson, R. E., Lanzerotti, L. J., Brown, W. L., Augustyniak, W. M., and Mussil, C.: 1983, *Astron. Astrophys.* **123**, 343–346.

Kobayashi, K., Kasamatsu, T., Kaneko, T., Koike, J., Oshima, T., Saito, T., Yamamoto, T., and Yanagawa, H.: 1995, *Adv. Space Res.* **16**, 21–26.

Le Beyec, Y.: 1992, in A. C. A. Souza, E. F. da Silveira, J. C. Nogueira, M. A. C. Nascimento and D. P. Almeidap (eds.), *Collision Processes of Ion, Positron, Electron and Photon Beams with Matter*, World Scientific, pp. 15–58.

Madey, T. E., Johnson, R. E., and Orlando, T. M.: 2002, *Surf. Sci.* **500**, 838–858.

Martinez, R., Ponciano, C. R., Farenzena, L. S., Iza, P., Homem, M. G. P., Naves de Brito, A., Wien, K. and da Silveira, E. F.: *Int. J. Mass Spectrom.* (In press).

Matsuo, T., Tonuma, T., Kumagai, H., Shibata, H., and Tawara, H.: 1994, *J. Chem. Phys.* **101**, 5356.

Moore, M. H., Khanna, R., and Donn, B.: 1991, *J. Geophys. Res.* **96**, 17541–17545.

Notesco, G., Bar-Nun, A., and Owen, T.: 2003, *Icarus* **162**, 183–189.

Pereira, J. A. M. and da Silveira, E. F.: 2000, *Phys. Rev. Lett.* **84**, 5904 .

Ponciano, C. R., Farenzena, L. S., Collado, V. M., da Silveira, E. F., and Wien, K.: 2005, *Int. J. Mass Spectrom.* **244**, 41–49.

Ponciano, C. R., Martinez, R., Farenzena, L. S., Iza, P., Homem, M. G. P., Naves de Brito, A., da Silveira, E. F. and Wien, K.: 2006, *J. Am. Soc. Mass Spectrom.* (In press).

SRIM-2003 code, Ziegler, J. F. and Biersack.: 1996, http://www.srim.org.

Strazzula, G. and Palumbo, M. E.: 1998, *Planet. Space Sci.* **46**, 1339–1348.

Strazzulla, G., Leto, G., Baratta, G. A., and Spinella, F.: 1991, *J. Geophys. Res.* **96**, 17547–17552.

Tawara, H., Tonuma, T., Kumagai, H., Matsuo, T., and Shibata, H.: 1991, *J. Chem. Phys.* **94**, 2730.

Tonuma, T., Kumagai, H., Matsuo, T., Shibata, H., and Tawara, H.: 1994, *Int. J. Mass Spectrom. Ion Processes* **135**, 129–137.

Wagner, M., Wien, K., Curdes, B., and Hilf, E. R.: 1993, *Nucl. Inst. & Meth. B* **82**, 362.

Wien, K.: 1997, *Nucl. Instr. & Meths. B* **131**, 38–54.